TEMPORAL VARIATION IN THE ORBITAL ELEMENT DISTRIBUTION OF THE 1998 LEONID OUTBURST

MARC C. DE LIGNIE, MARCO LANGBROEK, AND HANS BETLEM
Dutch Meteor Society, Lederkarper 4, 2318 NB Leiden, The Netherlands
E-mail: M.C.deLignie@planet.nl

and

PAVEL SPURNÝ
Astronomical Institute, Ondrejov Observatory, 251 65 Ondrejov, Czech Republic

(Received 10 July 2000; Accepted 7 September 2000)

Abstract. Double-station video observations of the 1998 Leonid shower from China resulted in 55 trajectories and orbits of meteoroids in the visual magnitude range from +0 to +6 magn. The 1998 Leonid outburst consisted of a relatively long duration shower that was rich in large meteoroids and peaked in the night of November 16/17, and an outburst of shorter duration that was rich in smaller meteoroids and peaked in the next night. The average orbit obtained during the first night agrees well with that from photographic observations. During the second night, the combined set of video and photographic observations shows temporal variation in the radiant distribution. This adds to the earlier discovery of an unusual asymmetric flux profile. In addition, the radiant distribution is shown to be mass dependent. The data suggest the presence of at least two merged dust components or a single dust component perturbed by planetary encounters.

Keywords: Leonids 1998, meteor, meteor shower, meteoroid, orbits, video

1. Introduction

With the increasing understanding of the dynamic evolution of fresh cometary ejecta a direct comparison between model studies and observations of meteor outbursts has become possible (Jenniskens, 1998). Dynamical simulations of the Leonid meteoroid stream (Kondrat'eva *et al.*, 1997; Asher *et al.*, 1999; Asher, 1999; Arlt and Brown, 1999) have aimed at reproducing observed meteor rate profiles. In this paper it is argued that the observed structure of the radiant area provides additional insight in the

Earth, Moon and Planets **82–83**: 295–304, 2000.

dust distribution of the Leonid meteoroid stream and can be used to validate model calculations.

In an earlier paper we reported on radiant structure on the basis of precise double-station photographic observations of the 1998 Leonid outbursts (Betlem *et al.*, 1999). In the present paper we extend this study using double-station video observations made of these same outbursts. With these observations we nearly double the sample of orbits of the 1998 outbursts. In addition we extend the magnitude range of the observed meteors to +6, allowing us to search more sensitively for mass dependent structure in the radiant area of the Leonid stream and thus to provide more stringent boundary conditions for model calculations to agree with.

2. Observations

Video observations were made at four locations in the Peoples Republic of China during three nights from November 16-18, 1998. The observations were part of a larger ground-based effort (Betlem *et al.*, 1999; Langbroek and De Lignie, 1999) that supported NASA's 1998 Leonid Multi-instrument Aircraft Campaign (Jenniskens and Butow, 1999). Locations were chosen in the areas of Xing Long (Hebei province) and Delingha (Qinghai province) such that stereoscopic observations could be made in two consecutive time zones. The Xing Long network covered the nights November 16 and 17, while the Delingha network covered the nights November 17 and 18. Exact geographic locations and camera details are listed in Table I. The video cameras typically consist of a second generation image intensifier and a Hi-8 or S-VHS camcorder. The field of view is about 25–40 degrees allowing for an astrometric resolution of 0.02 degree. The limiting magnitude for meteors is about +6 magn.

Deriving atmospheric trajectories and heliocentric orbits from the double-station video observations was done in a standard way described in (De Lignie, 1996). Magnitudes are estimated by visually comparing the surrounding stars on the video frame with the brightest meteor image. Corrections for distance were not made, but are typically smaller than 0.5 magnitude due to the high pointing elevation of the cameras.

Video observations of fast meteors only allow to measure average velocities along the trajectory. Therefore, pre-atmospheric entry velocities were estimated by adding 0.14 km/s to the measured average velocity, the value of 0.14 km/s being the typical difference between measured entry and average velocities for photographed meteors of that speed. This correction mainly influences the semi-major axis and has little effect on other orbital elements.

TABLE I

Location	Northern Latitude	Eastern Longitude	Camera type	Field (^{o})
Xing Long	40° 23’ 48”	117° 34’ 28”	2nd generation MCP + SVHS	25
Lin Ting Kou	39° 37’ 47”	117° 30’ 17”	2nd generation MCP + Hi-8	40
Delingha	37° 22’ 42”	97° 43’ 44”	3 stage 1st generation + Hi-8	28
Ulan	37° 08’ 52”	98° 23’ 48”	2nd generation MCP + Hi-8	28

3. Results

The full sample of 55 multi-station orbits is listed in Tables II and III. Seven of the 55 Leonids are from the night November 16/17, when an outburst of bright meteors was ramping up to a peak over Europe (Arlt, 1998; Jenniskens, 1999), while 46 are from the night of November 17/18 during passage of the node of comet Temple-Tuttle. In addition, two are from the following night of November 18/19.

Table II gives the orbital elements (J2000.0) of the 55 Leonid meteoroids. These are: the perihelion distance of orbit = q, semi-major axis = a, eccentricity = e. Node is short for the angle of ascending node and ω indicates the argument of perihelion of the orbit, while pi is Node + ω. Averages are listed separately for November 16 and 17. Meteors observed near Xing Long have video code numbers in the series that start with the numbers 982 and 983, while those observed near Delingha have codes starting with 984.

Table III gives the corresponding trajectory data (J2000.0). Velocity index G = geocentric, H = heliocentric, INF = topocentric before deceleration. Tolerances are given. Individual columns refer to beginning height (HB) and end height (HE) of the meteor, apparent radiant position and Geocentric radiant position. Z is the zenith distance of the radiant and Qmax is the angle between the two planes through stations and meteor trails. Again, averages are listed separately for November 16 and 17.

The basic parameters obtained from double-station observations are the geocentric radiant and entry velocity (direction and magnitude of the meteoroid’s velocity vector relative to the Earth). The velocity mainly affects the semi- major axis *a*. For the total sample, *a* averages 9.5 ± 1.3 AU, in agreement with the current semi-major axis of 10.3 AU for the parent comet 55P/Tempel-Tuttle.

TABLE II

code	day	Mv	q	tol	a	1/a	tol	e	tol	i	tol	w	tol	node	pi	tol
98224	16.7856	3	0.981	0.0012	50.0	0.020	0.07	0.980	0.068	162.8	0.4	169.9	0.9	234.23	44.1	0.9
98238	16.8062	3	0.985	0.0009	16.4	0.061	0.07	0.940	0.067	162.0	0.4	172.4	0.8	234.25	46.6	0.8
98245	16.8218	1	0.984	0.0009	64.2	0.016	0.07	0.985	0.068	161.8	0.4	171.9	0.8	234.27	46.2	0.8
98254	16.8437	0	0.984	0.0013	4.2	0.238	0.19	0.766	0.182	161.2	0.6	170.9	1.6	234.29	45.2	1.6
98259	16.8495	0	0.984	0.0009	19.8	0.050	0.07	0.950	0.067	162.3	0.4	171.7	0.8	234.29	46.0	0.8
98270	16.8711	3	0.983	0.0010	9.4	0.106	0.07	0.896	0.066	161.9	0.4	170.9	0.9	234.32	45.2	0.9
98278	16.8823	-1	0.986	0.0005	-13.0	-0.077	0.07	1.076	0.071	161.2	0.4	174.3	0.6	234.33	48.6	0.6
98297	17.6632	0	0.982	0.0009	11.7	0.085	0.07	0.916	0.067	163.5	0.4	170.3	0.8	235.11	45.4	0.8
98298	17.6643	2	0.984	0.0010	9.3	0.107	0.07	0.894	0.066	162.4	0.4	171.6	0.9	235.12	46.7	0.9
98308	17.7004	1	0.985	0.0007	36.8	0.027	0.07	0.973	0.068	161.5	0.4	173.2	0.8	235.15	48.4	0.8
98309	17.7030	5	0.984	0.0009	13.0	0.077	0.07	0.925	0.067	161.1	0.4	171.7	0.8	235.15	46.9	0.8
98315	17.7140	2	0.985	0.0008	5.9	0.170	0.07	0.833	0.064	161.8	0.4	172.4	0.8	235.17	47.5	0.8
98317	17.7170	2	0.983	0.0010	5.6	0.177	0.07	0.826	0.064	162.3	0.4	171.1	0.9	235.17	46.2	0.9
98319	17.7257	0	0.984	0.0009	39.7	0.025	0.07	0.975	0.068	163.3	0.4	171.9	0.8	235.18	47.1	0.8
98401	17.7275	3	0.980	0.0027	-5.6	-0.177	0.21	1.174	0.203	162.4	0.5	169.8	1.8	235.18	45.0	1.8
98321	17.7312	2	0.984	0.0010	9.1	0.109	0.07	0.892	0.066	161.9	0.4	171.8	0.9	235.18	47.0	0.9
98403	17.7355	4	0.980	0.0018	12.9	0.078	0.07	0.924	0.073	158.6	0.3	168.9	1.2	235.19	44.1	1.2
98333	17.7916	1	0.984	0.0010	5.3	0.190	0.06	0.814	0.064	162.0	0.4	171.6	0.9	235.24	46.8	0.9
98334	17.7927	2	0.983	0.0010	11.6	0.086	0.07	0.915	0.067	162.9	0.4	171.0	0.9	235.24	46.3	0.9
98415	17.8021	5	0.971	0.0060	8.6	0.116	0.19	0.887	0.181	160.7	0.7	164.2	3.2	235.25	39.4	3.2
98340	17.8026	2	0.984	0.0009	9.6	0.104	0.07	0.898	0.066	162.3	0.4	172.1	0.9	235.25	47.3	0.9
98341	17.8048	3	0.984	0.0009	-224.3	-0.004	0.07	1.004	0.069	163.0	0.4	171.8	0.8	235.26	47.1	0.8
98344	17.8072	2	0.984	0.0007	5.0	0.198	0.08	0.805	0.081	162.0	0.5	171.9	0.8	235.26	47.1	0.8
98417	17.8089	5	0.989	0.0002	107.6	0.009	0.07	0.991	0.069	163.8	0.3	179.1	1.2	235.26	54.4	1.2
98418	17.8115	3	0.985	0.0011	15.9	0.063	0.07	0.938	0.071	162.3	0.3	172.4	1.0	235.26	47.7	1.0
98419	17.8145	5	0.984	0.0042	2.2	0.460	0.21	0.548	0.202	162.7	0.8	170.2	4.6	235.27	45.5	4.6
98424	17.8285	1	0.986	0.0009	33.3	0.030	0.07	0.970	0.068	162.3	0.3	173.7	1.0	235.28	48.9	1.0
98426	17.8316	5	0.967	0.0053	4.2	0.238	0.10	0.770	0.099	161.7	0.5	161.9	2.6	235.28	37.2	2.6
98428	17.8342	4	0.984	0.0014	4.0	0.247	0.13	0.757	0.127	162.0	0.4	171.5	1.5	235.29	46.7	1.5
98429	17.8416	2	0.986	0.0009	33.3	0.030	0.07	0.970	0.068	163.0	0.3	173.7	1.0	235.29	48.9	1.0
98357	17.8422	6	0.985	0.0010	5.8	0.174	0.10	0.829	0.099	162.6	0.4	172.6	1.1	235.29	47.9	1.1
98430	17.8447	1	0.986	0.0009	15.7	0.064	0.07	0.937	0.067	162.3	0.3	173.4	1.0	235.30	48.7	1.0
98359	17.8448	1	0.984	0.0010	10.7	0.093	0.12	0.908	0.117	162.3	0.4	172.0	1.0	235.30	47.3	1.0
98431	17.8449	4	0.985	0.0011	9.9	0.101	0.07	0.901	0.066	163.1	0.3	172.6	1.1	235.30	47.9	1.1
98360	17.8450	-1	0.985	0.0008	20.7	0.048	0.07	0.952	0.068	162.8	0.4	172.7	0.8	235.30	47.9	0.8
98362	17.8467	3	0.985	0.0008	-53.2	-0.019	0.07	1.019	0.070	162.7	0.4	173.4	0.8	235.30	48.7	0.8
98369	17.8537	4	0.982	0.0017	12.3	0.081	0.10	0.920	0.099	163.1	0.6	170.6	1.4	235.31	45.9	1.4
98435	17.8537	3	0.983	0.0012	15.4	0.065	0.07	0.936	0.067	161.6	0.3	170.9	1.0	235.31	46.2	1.0
98436	17.8547	-1	0.984	0.0017	2.7	0.370	0.19	0.636	0.191	162.0	0.5	171.2	2.2	235.31	46.5	2.2
98370	17.8556	5	0.980	0.0014	5.6	0.177	0.08	0.826	0.074	163.5	0.4	168.6	1.0	235.31	43.9	1.0
98437	17.8565	2	0.985	0.0011	-70.1	-0.014	0.18	1.014	0.175	162.4	0.4	172.8	1.2	235.31	48.1	1.2
98373	17.8585	6	0.983	0.0014	3.1	0.321	0.10	0.685	0.097	162.7	0.4	170.0	1.4	235.31	45.3	1.4
98374	17.8586	2	0.985	0.0008	-17.4	-0.058	0.07	1.057	0.070	162.4	0.4	173.3	0.8	235.31	48.6	0.8
98380	17.8643	3	0.986	0.0007	-36.6	-0.027	0.07	1.027	0.070	162.5	0.4	173.6	0.8	235.32	48.9	0.8
98442	17.8730	3	0.985	0.0012	7.1	0.140	0.12	0.862	0.120	163.1	0.4	172.8	1.3	235.33	48.1	1.3
98443	17.8735	3	0.984	0.0015	4.2	0.237	0.18	0.767	0.178	162.5	0.5	171.2	1.7	235.33	46.5	1.7
98444	17.8735	3	0.985	0.0015	4.7	0.213	0.24	0.790	0.239	161.9	0.6	172.1	1.9	235.33	47.4	1.9
98390	17.8792	2	0.985	0.0008	11.8	0.085	0.08	0.917	0.077	162.2	0.5	172.5	0.8	235.33	47.9	0.8
98445	17.8817	0	0.984	0.0010	5.5	0.183	0.08	0.820	0.075	162.5	0.4	172.1	1.0	235.33	47.4	1.0
98394	17.8878	2	0.984	0.0009	7.0	0.142	0.07	0.860	0.065	162.5	0.4	171.9	0.9	235.34	47.2	0.9
98395	17.8878	5	0.985	0.0007	26.4	0.038	0.07	0.963	0.068	162.5	0.4	172.9	0.7	235.34	48.2	0.7
98397	17.8892	-1	0.986	0.0006	-7.1	-0.142	0.07	1.140	0.073	162.5	0.4	174.0	0.7	235.34	49.3	0.7
98398	17.9014	0	0.986	0.0008	46.0	0.022	0.07	0.979	0.068	162.8	0.4	173.5	0.8	235.35	48.9	0.8
98457	17.9512	1	0.983	0.0009	3.2	0.317	0.10	0.688	0.099	162.1	0.5	170.7	1.1	235.40	46.1	1.1
98458	17.9522	4	0.981	0.0014	3.1	0.319	0.10	0.687	0.097	162.6	0.5	168.9	1.3	235.41	44.3	1.3
98467	18.8207	3	0.968	0.0116	1.7	0.574	0.29	0.445	0.273	160.2	0.9	158.8	10.5	236.28	35.1	10.5
98472	18.8573	3	0.988	0.0004	-12.5	-0.080	0.15	1.079	0.146	161.7	0.4	177.5	1.0	236.32	53.8	1.0
average	16.84	1.3	0.984		16.9	0.059		0.942		161.9		171.7		234.28	46.0	
st. dev	0.03	1.7	0.002			0.097		0.095		0.6		1.4		0.04	1.4	
average	17.82	2.4	0.983		8.9	0.112		0.890		162.3		171.6		235.27	46.9	
st. dev	0.07	1.8	0.003			0.124		0.122		0.8		2.5		0.07	2.5	

TABLE III

code	VG	VH	VINF	<V>	tol	HB	Hmax	HE	RA	tol	DE	tol	RAG	DEG	cos Z	Qmax
98224	71.4	42.1	72.6	72.4	0.7	128.1	108.1	99.5	153.29	0.24	21.81	0.21	153.41	21.72	0.622	48
98238	71.0	41.7	72.1	71.9	0.7	127.8	113.3	97.4	152.77	0.22	22.46	0.22	152.82	22.38	0.706	54
98245	71.4	42.2	72.5	72.4	0.7	138.3	104.8	94.3	153.10	0.21	22.54	0.23	153.10	22.46	0.754	60
98254	69.0	39.8	70.1	69.9	2.1	125.5	101.8	91.9	153.12	0.19	22.62	0.24	153.05	22.55	0.820	90
98259	71.1	41.8	72.1	72.0	0.7	132.3	104.5	91.9	153.09	0.23	22.21	0.21	153.00	22.14	0.831	83
98270	70.5	41.2	71.5	71.3	0.7	123.0	109.7	99.8	153.38	0.22	22.32	0.22	153.23	22.24	0.879	79
98278	72.3	43.2	73.3	73.2	0.7	153.6	122.3	109.4	152.90	0.19	23.14	0.25	152.72	23.08	0.905	57
98297	70.8	41.5	72.0	71.9	0.7	124.0	117.6	116.7	153.31	0.15	21.36	0.27	153.87	21.06	0.103	35
98298	70.5	41.2	71.7	71.6	0.7	118.9	116.4	113.0	153.14	0.26	22.06	0.19	153.71	21.77	0.116	36
98308	71.3	42.1	72.5	72.3	0.7	122.1	113.3	109.4	153.21	0.21	22.61	0.23	153.63	22.42	0.282	39
98309	70.7	41.6	71.9	71.8	0.7	125.9	118.0	114.2	153.66	0.19	22.69	0.24	154.09	22.49	0.289	38
98315	69.8	40.5	71.0	70.9	0.7	112.9	109.1	98.2	153.17	0.19	22.29	0.24	153.56	22.11	0.343	48
98317	69.7	40.5	71.0	70.8	0.7	112.1	109.1	100.1	153.39	0.22	21.89	0.22	153.77	21.71	0.349	48
98319	71.5	42.1	72.6	72.5	0.7	133.4	-	108.1	153.30	0.20	21.50	0.23	153.64	21.34	0.382	41
98401	73.4	44.2	74.6	74.5	2.1	127.1	123.0	120.6	154.32	0.57	21.85	0.14	154.85	21.62	0.126	18
98321	70.4	41.2	71.6	71.5	0.7	123.8	111.4	100.0	153.51	0.24	22.15	0.21	153.83	21.99	0.410	46
98403	70.4	41.5	71.6	71.5	0.8	119.0	116.4	111.7	154.97	0.36	23.70	0.09	155.52	23.47	0.176	23
98333	69.6	40.3	70.7	70.6	0.7	118.1	110.6	97.6	153.66	0.22	21.99	0.22	153.77	21.89	0.654	61
98334	70.8	41.5	71.9	71.8	0.7	121.5	114.5	102.5	153.82	0.22	21.48	0.22	153.92	21.39	0.649	49
98415	70.2	41.1	71.4	71.2	2.0	114.0	111.1	106.0	155.95	0.78	21.90	0.16	156.24	21.78	0.456	26
98340	70.5	41.3	71.7	71.5	0.7	122.9	114.6	99.1	153.67	0.23	21.87	0.21	153.73	21.78	0.690	54
98341	71.7	42.4	72.8	72.7	0.7	125.4	107.8	101.5	153.81	0.23	21.56	0.22	153.86	21.48	0.693	50
98344	69.5	40.2	70.6	70.5	0.9	120.7	108.6	96.3	153.63	0.13	21.99	0.28	153.68	21.90	0.709	65
98417	71.7	42.3	72.9	72.7	0.7	120.4	115.0	106.5	151.30	0.41	21.86	0.09	151.50	21.77	0.537	26
98418	71.0	41.7	72.2	72.0	0.8	122.5	110.5	93.3	153.51	0.31	21.94	0.09	153.73	21.85	0.523	26
98419	66.6	37.2	67.8	67.7	2.4	118.2	115.2	109.1	153.00	0.85	21.41	0.17	153.25	21.30	0.537	25
98424	71.3	42.0	72.5	72.4	0.7	124.6	110.0	95.4	153.28	0.31	22.07	0.10	153.44	21.99	0.598	39
98426	68.9	39.8	70.1	70.0	1.1	116.1	108.5	105.7	155.97	0.61	21.15	0.14	156.16	21.05	0.573	30
98428	69.0	39.7	70.1	70.0	1.4	122.8	106.5	98.4	153.56	0.32	21.93	0.07	153.71	21.85	0.617	35
98429	71.4	42.0	72.5	72.4	0.7	124.2	110.9	99.9	153.19	0.31	21.68	0.09	153.29	21.61	0.646	34
98357	69.8	40.5	70.9	70.8	1.1	117.3	114.1	105.6	153.50	0.26	21.73	0.17	153.43	21.65	0.814	71
98430	71.0	41.7	72.1	72.0	0.7	132.2	108.8	96.5	153.40	0.31	22.04	0.10	153.50	21.98	0.659	37
98359	70.7	41.4	71.7	71.6	1.3	127.3	110.8	97.2	153.90	0.22	21.86	0.22	153.83	21.79	0.817	63
98431	70.7	41.3	71.8	71.7	0.7	115.7	112.1	102.6	153.36	0.32	21.48	0.10	153.46	21.40	0.657	37
98360	71.2	41.9	72.2	72.1	0.7	138.5	111.9	93.5	153.69	0.23	21.71	0.21	153.62	21.64	0.817	58
98362	71.9	42.6	72.9	72.8	0.7	127.7	115.3	101.5	153.62	0.24	21.86	0.20	153.54	21.79	0.823	59
98369	70.9	41.5	71.9	71.8	1.1	103.6	101.2	98.0	154.14	0.37	21.27	0.32	154.05	21.19	0.835	77
98435	70.9	41.7	72.0	71.9	0.7	114.5	98.1	92.6	154.29	0.29	22.13	0.13	154.37	22.07	0.686	52
98436	67.6	38.3	68.8	68.6	2.2	131.3	99.6	91.6	153.43	0.30	21.81	0.10	153.50	21.74	0.695	46
98370	69.8	40.5	70.9	70.7	0.8	120.3	112.6	103.3	154.37	0.22	20.87	0.22	154.27	20.78	0.833	53
98437	71.8	42.5	72.9	72.8	1.9	129.8	106.8	98.8	153.73	0.30	21.95	0.11	153.79	21.89	0.699	41
98373	68.2	38.9	69.3	69.1	1.1	125.6	106.0	103.4	153.83	0.25	21.35	0.19	153.72	21.26	0.848	70
98374	72.2	43.0	73.3	73.1	0.7	126.0	113.0	97.7	153.81	0.25	22.04	0.19	153.70	21.97	0.852	67
98380	71.9	42.6	73.0	72.8	0.7	125.2	107.4	97.1	153.68	0.24	22.02	0.20	153.54	21.94	0.866	71
98442	70.2	40.9	71.3	71.2	1.3	126.6	110.3	105.7	153.37	0.35	21.49	0.16	153.37	21.43	0.758	43
98443	69.1	39.8	70.2	70.1	2.0	118.4	107.2	98.6	153.73	0.29	21.60	0.13	153.73	21.54	0.757	58
98444	69.3	40.1	70.5	70.3	2.7	123.2	109.7	104.5	153.68	0.30	21.99	0.13	153.69	21.93	0.757	41
98390	70.7	41.5	71.7	71.6	0.8	119.9	110.1	102.3	153.92	0.20	21.98	0.26	153.75	21.90	0.893	63
98445	69.7	40.4	70.8	70.7	0.8	129.9	106.5	93.4	153.65	0.24	21.70	0.20	153.62	21.64	0.783	86
98394	70.2	40.8	71.1	71.0	0.7	124.0	111.7	94.7	153.97	0.23	21.74	0.21	153.77	21.65	0.906	81
98395	71.3	42.0	72.2	72.1	0.7	119.2	104.2	91.9	153.85	0.20	21.85	0.23	153.65	21.77	0.908	75
98397	73.1	43.8	74.1	73.9	0.7	145.4	99.9	98.3	153.78	0.22	22.08	0.22	153.59	22.01	0.910	59
98398	71.5	42.1	72.4	72.3	0.7	133.2	109.1	95.9	153.69	0.25	21.81	0.20	153.47	21.72	0.925	69
98457	68.2	38.9	69.2	69.0	1.1	130.4	102.7	90.1	154.05	0.13	21.70	0.28	153.81	21.63	0.936	62
98458	68.2	38.9	69.2	69.0	1.1	125.3	110.0	101.4	154.35	0.18	21.27	0.25	154.12	21.20	0.933	54
98467	64.9	35.9	66.2	66.0	3.6	114.7	110.3	101.3	156.11	0.33	21.52	0.10	156.37	21.40	0.541	32
98472	72.4	43.2	73.5	73.4	1.5	107.7	96.6	94.4	153.56	0.34	22.53	0.11	153.60	22.48	0.717	52
average	71.0	41.7	72.0	71.9		132.7	109.2	97.7	153.09		22.44		153.05	22.37		
st. dev	1.0	1.0	1.0	1.0		10.5	6.9	6.1	0.21		0.41		0.24	0.41		
average	70.4	41.2	71.6	71.4		123.4	110.2	101.2	153.73		21.84		153.83	21.73		
st. dev	1.3	1.3	1.3	1.3		7.1	5.0	6.8	0.69		0.44		0.71	0.42		

Since the radiant coordinates can be determined with much greater precision than the entry velocity, these parameters are most suitable to look for structure in the distribution of meteoroid orbits. Figure 1 shows the observed radiant points, together with the photographically observed radiant points from Betlem *et al.* (1999). In this diagram the radiant points are corrected for the daily motion of the radiant due to the changing velocity vector of the Earth. This correction amounts to +0.99 and –0.36 degree per degree of solar longitude for the right ascension and declination, respectively. The correction was applied towards the arbitrary value of 235.0 degrees of solar longitude.

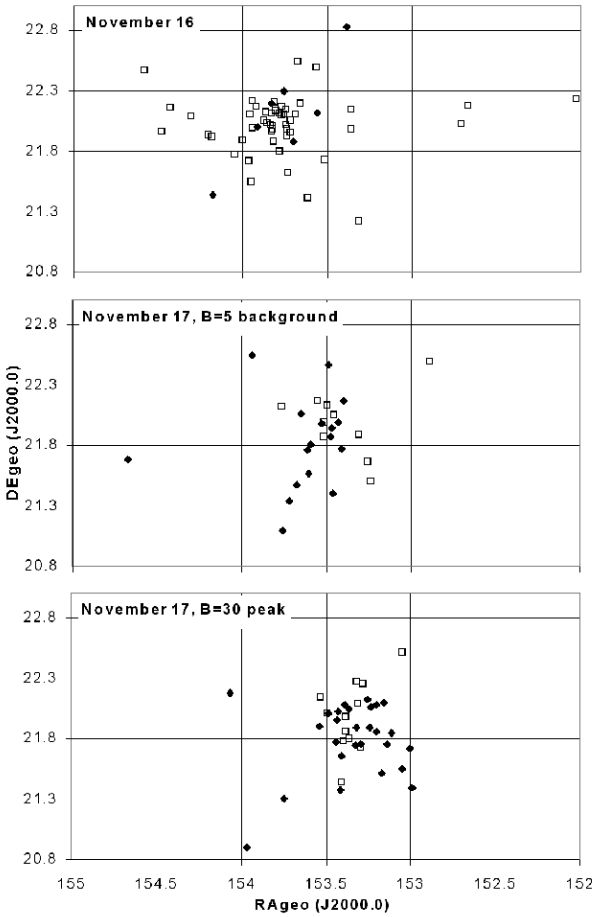

Figure 1. Radiant areas observed during the November 16 and 17 Leonid outbursts with all points moved to solar longitude 235.00 degrees. Closed diamonds refer to video observations, while open squares refer to photographic observations from Betlem *et al.* (1999).

In Figure 1, the radiant points of Nov. 16 are drawn separately, while in addition the sample of Nov. 17 is subdivided in a sample containing the radiant points observed between solar longitudes 235.27 and 235.36 degrees and a sample covering the remaining ranges of solar longitude. The subdivision of the Nov. 17 sample was chosen in line with the earlier discovery of an unusual asymmetric rate profile (Langbroek and De Lignie, 1999; Jenniskens, 1999). The rate profile was shown to be fitted well with a sum of two symmetric exponential distributions with maxima at solar longitudes 235.260 and 235.316 and steepness B = 5 and B = 30, respectively. We now find that the radiant coordinates observed during this proposed B = 30-peak have a systematically smaller right ascension than the radiant coordinates of the B = 5-peak. Note that this difference is problably even larger than visible from the diagram, because during the activity of the B = 30-peak, the B = 5-peak still contributed about 50% of activity.

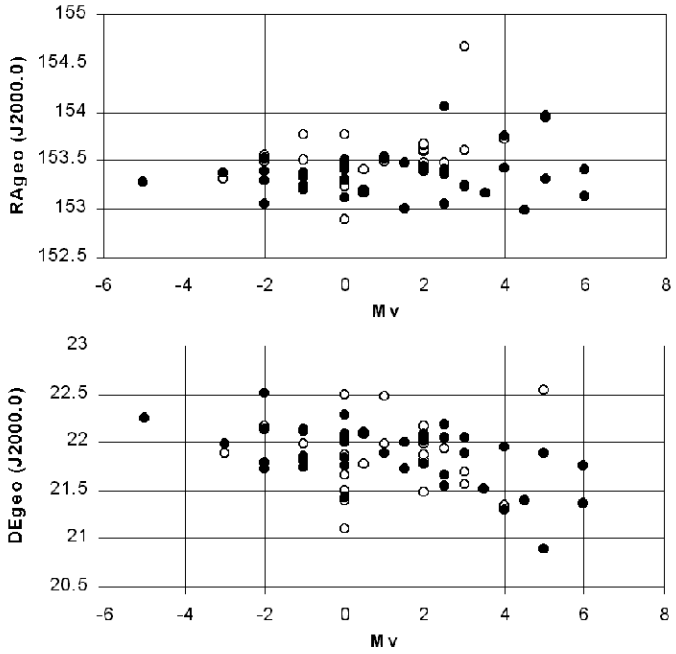

Figure 2. Radiant coordinates as a function of absolute visual magnitude of both the video and photographic observations of November 17 (the data sets only overlap for Mv=0). Open dots: B=5 structure. Filled dots: B=30 narrow peak.

In the B = 30 radiant diagram for November 17, the video and photographic observations do not perfectly coincide, as the video radiants

TABLE IV

Component	Source	N	RA_{geo}	DE_{geo}
Nov 16	Video	7	153.76 ± 0.10	22.11 ± 0.16
Nov 16	Photo	51	153.80 ± 0.06	22.05 ± 0.03
Nov 17, B=5	Video	17	153.57 ± 0.07	21.82 ± 0.09
Nov 17, B=5	Photo	10	153.46 ± 0.08	21.93 ± 0.09
Nov 17, B=30	Video	27	153.35 ± 0.05	21.80 ± 0.06
Nov 17, B=30	Photo	12	153.35 ± 0.04	21.99 ± 0.08

have a slightly smaller declination on average. As indicated in Table 4 the difference is about 0.19 degrees, which is just on the edge of statistical significance. Figure 2 gives a more detailed view of the mass dependence of the radiant coordinates during the nodal outburst activity of November 17. This way of presenting the data visualizes a small but significant mass dependent correlation between the visual magnitude and the declination of the radiant points of the B = 30 peak. The right ascension of the B=30 peak and the radiant coordinates of the B=5 peak might also have a small mass dependence, but if present it is hidden in the dispersion of the radiant distribution.

Finally, one can see that the average position of the radiants obtained from video observations during Nov. 16, coincides with the photographic one (Betlem *et al.*, 1999). As pointed out before, the radiant is different from that of the Nov. 17/18 outburst. Table IV gives average radiants and standard errors, with all radiants moved to solar longitude 235.00 degrees. The outliers with video code numbers 98370, 98401, 98403, 98415, 98417 and 98426 were not included in these values.

4. Discussion

The newly obtained data allow for a review of possible associations between theoretically proposed structures in the Leonid stream and the three dust components observed in 1998. Existing models discriminate between young single ejecta from the parent comet, old single ejecta trapped in an orbital resonance, the so-called Leonid filament consisting of multiple ejecta (Jenniskens and Betlem, 2000) and the annual stream.

According to dynamical simulations of the Leonid meteoroid stream (Kondrat'eva *et al.*, 1997; Asher *et al.*, 1999; Asher, 1999; Arlt and Brown, 1999) the nearest single ejecta dust trail to the Earth's orbit in 1998 was that of dust ejected in 1899. However, it was thought that the Earth had created a gap in the dust distribution during its previous encounter in 1965 and no outburst was expected (McNaught and Asher, 1999). The younger trail ejected in 1932 was significantly further away from Earth.

It is shown in Asher *et al.* (1999) that parts of single ejecta can survive perturbations by the major planets during many revolutions, when trapped in orbital resonances with the major planets. In particular, it was shown by model calculations that a resonance part of the ejecta of 1333 would be visible in 1998.

In Jenniskens and Betlem (2000) the so-called Leonid Filament was proposed, which is visible in the years around perihelion passage of 55P/Tempel-Tutle. The filament is populated by the ejecta of multiple perihelion passages of the comet, but has nevertheless a finite extent due to small ejection velocities in combination with protection against planetary perturbations due to the comet's orbit close to the 5:14 resonance with Jupiter and the 8:9 resonance with Saturn.

The association of the three observed dust components in 1998 with these theoretical structures is not straightforward. In Jenniskens and Betlem (2000), the Nov. 16 fireball outburst was associated with the Leonid filament. In this interpretation the B = 5 and B = 30 outbursts of Nov. 17 are associated with the recent 1899 or 1932 ejecta. Arguments in favor of this association scheme are the corresponding durations and mass distributions of the 1994–1997 outbursts and the Nov. 16 outburst. However, the deviating node of the Nov. 16 outburst and the occurrence of a rather wide B = 5 outburst from a single ejecta are not easily accounted for. This would require explanations in terms of planetary perturbations such as the 1965 encounter of the 1899 ejecta with the Earth.

In an alternative scheme of associations, the Nov. 16 outburst is associated with the 1333 resonant structure (Asher *et al.*, 1999), the B = 5 Nov. 17 outburst is associated with the Leonid filament and the B = 30 outburst is associated with a recent ejecta. Arguments in favor of this scheme are the similar node and radiant positions of the 1995–1997 outbursts and the B = 5 component of Nov. 17. However, the 1994 outburst showed that significant deviations between the filament and the node of the comet are possible. Additionally, the outbursts of 1994–1997 were much wider (B = 1) and richer in large particles than the B = 5 outburst of 1998. On the other hand, width and mass distribution of the filament might depend on the position relative to the comet.

In either association scheme the observed mass dependence in the radiant distribution of the B = 30 peak could be the result of the original mass dependent ejection velocity distribution from the parent comet in combination with the differences in evolution due to radiation pressure and the required intersection with the Earth's orbit.

5. Summary

The double-station video observations of the 1998 Leonid outbursts extend the picture obtained from earlier reported photographic observations. Temporal variations in the radiant distribution were shown to correspond to

features in the activity rate curves, which corresonds to the nodal distribution of orbits. Associations between observed dust components and theoretically modelled structures in the Leonid stream cannot be made unambiguously. It is made plausible that in the combined set of video and photographic observations, a small mass-dependence is present in the November 17 B = 30 radiant distribution. It is suggested that this mass dependence derives from the original ejection process at the parent comet.

Acknowledgements

We thank referee David Asher and Peter Jenniskens for their helpful comments in improving the paper. Klaas Jobse, Casper ter Kuile and Romke Schievink made an essential contribution to the achieved results by building and operating the video cameras. Carl Johannink and Koen Miskotte made a large effort in speeding up the data reduction. Dr. Guangyu Li, Dr. Jin Zhu, Dr. Chengming Lei and Dr. Haibin Zhao from Purple Mountain Observatory enabled the expedition by providing overall coordination of transport, lodging facilities and import. Financial funding was made available by the Royal Dutch Academy of Sciences (KNAW), the NASA Planetary Astronomy program, the Dutch Physics Foundation (Stichting Physica), the Leids Kerkhoven-Bosscha Fonds (KBF) and air cargo company Ufreight from Amsterdam Schiphol. Material support was provided by Kodak Netherlands and Canon Benelux. *Editorial handling*: Peter Jenniskens.

References

Asher, D.J.: 1999, *MRNAS* **307**, 919–924.

Asher, D.J., Bailey, M.E., and Emel'yanenko, V.V.: 1999, *MNRAS* **304**, L53–L56.

Arlt, R.: 1998, WGN, *Journal of the IMO*, **26**, 239–248.

Arlt, R. and Brown, P.: 1999, *WGN, Journal of the IMO*, **27**, 267–285.

Betlem, H., Jenniskens, P., Leven, J. van `t, Kuile, C. ter, Johannink, C., Haibin, Zhao, Chengming Lei, Guangyu Li, Jin Zhu, Evans S., and Spurny, P.: 1999, Meteorit. Planet. Sci. **34**, 979–986.

De Lignie, M. and Jobse, K.: 1996, *WGN, Journal of the IMO*, **24**, 20–26.

Jenniskens, P.: 1998, *Earth Planets Space* **50**, 555–567.

Jenniskens, P.: 1999, *Meteorit. Planet. Sci.* **34**, 959-968.

Jenniskens, P. and Butow S.J.: 1999, *Meteorit. Planet. Sci.* **34**, 933–943.

Jenniskens, P. and Betlem, H.: 2000, *Astrophys. J.* **531**, 1161–1167.

Kondrat'eva, E.D., Murav'eva, I.N., and Reznikov, E.A.: 1997, *Sol. Syst. Res.* **31**, 489–492.

Langbroek, M. and De Lignie, M.: 1999, *WGN, Journal of the IMO*, **27**, 30–32.

McNaught R. and Asher, D.J. : 1999, *WGN, Journal of the IMO*, **27**, 85–102.